# Design of Modular High Temperature Sodium Solar Collection Subsystems

Daniel Potter[1] (iD) and Yen Chean Soo Too[1]

[1] CSIRO, Australia

**Abstract.** Optimised designs of 11.7MW$_{th}$ solar collection subsystem modules based on high temperature (740°C) sodium central receivers are investigated. Billboard and cavity receivers mounted on steel lattice towers are considered, and radially staggered and Cartesian heliostat field layouts are compared. A billboard receiver paired with a Cartesian heliostat field layout was found to give the overall lowest levelised cost of heat (LCOH), albeit with a significantly taller tower compared to using a radially staggered heliostat field layout.

**Keywords:** Sodium, Heliosim, Optimisation, Modular

## 1. Introduction

High temperature (>700°C) liquid sodium solar receivers have been identified as a possible pathway towards next generation concentrating solar power (CSP) facilities that utilise high efficiency power cycles such as the supercritical carbon dioxide Brayton cycle [1]. Whilst current nitrate salt CSP systems typically consist of large ($\gtrsim$50MW$_{th}$) cylindrical receivers with surround heliostat fields, an alternative configuration is a collection of smaller solar collection subsystem (SCS) modules connected with insulated pipe networking to centralised storage and power generation. This multi-tower concept has been successfully demonstrated by Vast Solar for lower temperature (≈560°C) sodium [2]. It allows increased flexibility of the overall system scalability and operation, along with increased solar collection efficiency. Furthermore, smaller receivers can take advantage of using relatively inexpensive steel lattice towers. These benefits, however, must be weighed against the additional costs and losses of the extensive horizontal pipe networking from each module to the centralised storage location.

Whilst cylindrical receivers with surround fields have been found to give good performance for high temperature sodium SCS with thermal capacities from 175 to 700MW$_{th}$ [3], billboard and cavity receivers with polar fields are more suited to smaller module capacities where proportionally taller towers can be used to reduce the rim angle. The Australian Solar Thermal Research Institute (ASTRI) has designed, constructed, and commenced on-ground commissioning of a 700kW$_{th}$ prototype sodium receiver [4]. This receiver consists of two independent sodium flow paths, each consisting of 5 vertical tube banks connected in series by a serpentine arrangement, enclosed in a cavity with a circular aperture. A 1MW$_{th}$ pilot-scale billboard sodium receiver was designed using a similar flow path concept for the Gen3 Liquid-Phase Pathway to SunShot project [1]. The ASTRI cavity receiver is on schedule to commence on-sun commissioning and operation at CSIRO Newcastle in late 2023.

As part of the ASTRI Thermal Energy Systems program, 10 to 50MW$_e$ CSP plants were designed using the multi-tower concept with high temperature sodium (740°C) as the receiver heat transfer fluid (HTF), thermally conductive graphite as the storage medium, and a dry-

cooled recompression $sCO_2$ Brayton cycle as the power block. In the present work, the design of the nominal 11.7MW$_{th}$ SCS module using the CSIRO's Heliosim software [5] is presented.

# 2. Methodology

The scope of the present work is the LCOH-based optimisation of a single SCS module and is illustrated in the context of the complete plant design workflow in Figure 1. The SCS consists of the receiver, tower, and heliostat field, however the design of these subsystems is tightly coupled to the overall system design (e.g. the land footprint of the SCS constrains the pipe networking design). Due to this coupling, all plant subsystems would ideally be optimised based on LCOE. The accurate design of high temperature tubular sodium receivers, however, requires complex and computationally intensive optics, heat transfer, and tube stress simulations that makes such an approach difficult to implement. The SCS design in the present work was therefore decoupled from the complete plant design by optimising on an LCOH basis with pipe networking cost per module incorporated in an approximate manner.
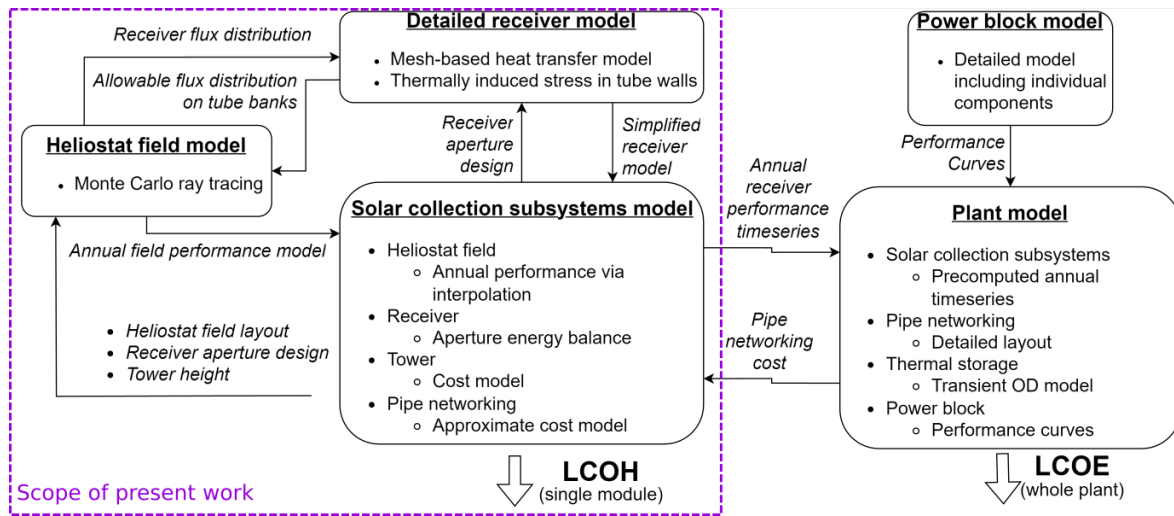


***Figure 1.*** *Scope of the present work in the context of the complete plant design workflow.*

It should be noted that, in the present work, LCOH is defined as the levelised cost of thermal energy captured by the receiver of a single module where the capital cost does not include balance of plant, storage or power block. Whilst this definition of LCOH is the same as calculated by the SolarPILOT software (e.g. as used in the analyses of Zhu et al. [6]), it is different from that used for the analysis of CSP systems for process heat applications (e.g. [7] and [8]). Comparing the quantified LCOH values presented here with other works should therefore be done with care.

## 2.1 Design parameters

The key design parameters for the case study are summarised in Table 1. The site is Tom Price in the Pilbara region of Western Australia and was selected due to its high annual insolation (2738 kWh/m$^2$), proximity to industry with a wide range of energy requirements, and remote location relative to the electricity grid. 11.7MW$_{th}$ billboard or cavity sodium receivers mounted on steel truss towers with radially staggered or polar cartesian heliostat field layouts are considered. The choice between these receiver and heliostat field layout designs is a key aspect of the present work, and the modelling for each is further described in the following sections. A small 2.25 × 2.25m heliostat based on the CSIRO's patented tilt-roll design is considered, with an effective slope error of 1.5mrad and specular reflectance of 0.9. Costing of site improvements, heliostat field and land are equal to the values used in the Gen3 liquid pathway project [1]. The receivers are also costed based on the Gen3 liquid pathway work by

converting the absorber tube arrangement for the billboard and cavity receivers to a cylindrical equivalent, with the cavity receiver incurring a 15% increase to account for the additional insulation, casing, and shielding costs. The cost of steel lattice towers is based on the correlation derived by Rea et al. [9] from a survey of wind turbine tower literature, with the tower load for the 11.7MW$_{th}$ receivers conservatively set to 10T. The pipe networking cost is assumed to be proportional to the east-west extent of the SCS module land footprint and the value of 5100 USD/m is based on a detailed pipe networking design for a 30MW$_e$ system. O&M costs are not considered as they are usually calculated on a system electrical capacity basis and would therefore not influence the design of the SCS module, however it is acknowledged that some O&M costs such as that for heliostat cleaning should be proportional to heliostat field size and could be included as such in future work.

*Table 1. Key design parameters considered in the present work.*

| Site | |
|---|---|
| Location | Tom Price, WA (-22.6234°,117.8672°) |
| Weather data | TMY file from NSRDB v3.0.1 |
| Design point | Equinox solar noon with DNI of 980W/m$^2$ |
| **Receiver** | |
| Thermal capacity (MW) | 11.7 |
| Heat transfer medium | Liquid sodium in tubes |
| Receiver design | a)  Square billboard<br>b)  Cavity with circular aperture |
| Sodium inlet & outlet temperatures (°C) | 480 & 740 |
| Tube material | Inconel Alloy 740H (UNS N07740) |
| Tube coating | Next generation high solar absorptivity coating [10] |
| Sodium velocity limit (m/s) | 3 [1] |
| Tube stress limit | ASME BPVC Section VIII Div. 2 |
| **Heliostat field** | |
| Heliostat design | 2.25 × 2.25m tilt-roll |
| Heliostat effective slope error (mrad) | 1.5 |
| Layout pattern | a)  Radially staggered with dense inner zone<br>b)  Cartesian with linearly varying spacing |
| **Tower** | |
| Design | Steel lattice |
| Cost model | Correlation from Rea et al. [9] with 10T load |
| **Pipe networking** | |
| Hot side | Inconel Alloy 740H with insulation and heat tracing |
| Cold side | Stainless steel 347H with insulation and heat tracing |

## 2.2 Receiver modelling

The billboard and cavity receiver concepts are illustrated in Figure 2 and Figure 3, respectively. Both receivers consist of two flow paths with independently controlled mass flow rates and are allowed to be tilted down from the horizon at an optimised elevation angle. A particular constraint of the cavity receiver design is that all heliostats are aimed at the aperture centroid, with the beams then diverging to form a distribution on the absorber tube banks positioned some distance behind. Whilst the billboard receiver allows a multi-aimpoint strategy to accurately control the level of solar flux on the absorber tubes, the cavity receiver relies on the cavity depth, tube length and degree of tube bank concavity being appropriately designed.
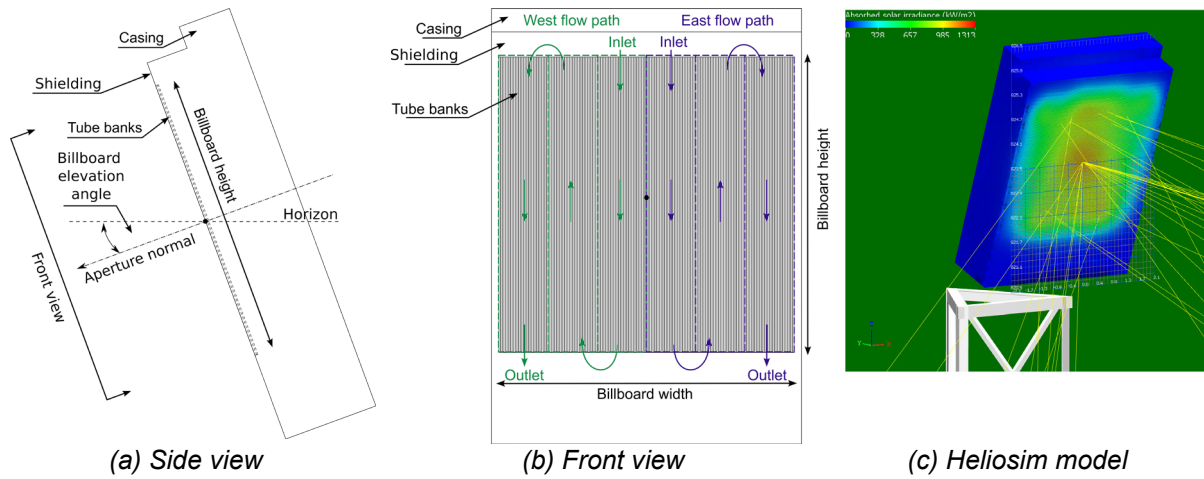
*(a) Side view*          *(b) Front view*          *(c) Heliosim model*

**Figure 2.** *Billboard sodium receiver concept.*



*(a) Cutaway view*          *(b) Side view*          *(c) Heliosim model*
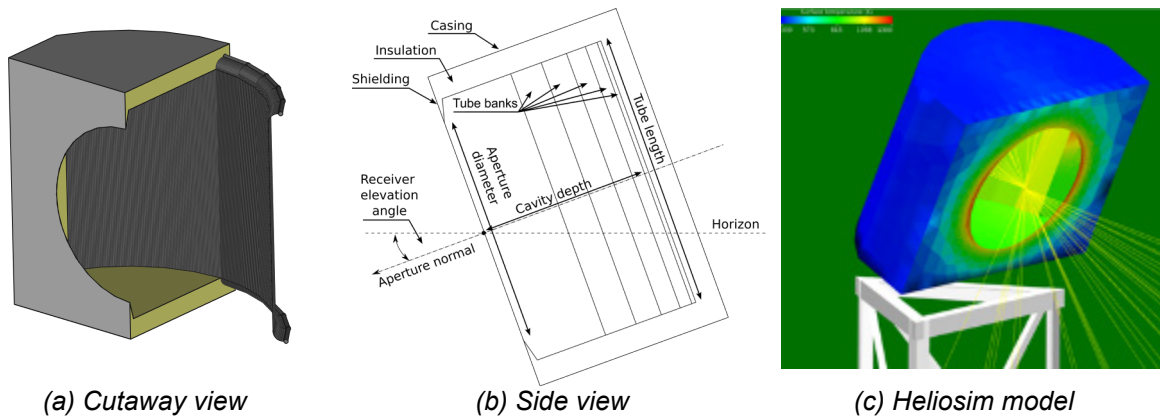
**Figure 3.** *Cavity sodium receiver concept.*

For both receiver concepts, the solar flux incident on the tube banks is limited to ensure the thermally induced stress in the absorber tubes is kept below the 100,000h limit specified by the elastic ratchet analysis method (i.e. the 'twice yield' method) from ASME BPVC Section VIII Div. II. The maximum sodium velocity of 3m/s also imposes a constraint on absorber tube design. Both constraints are plotted for various tube sizes suitable for a billboard receiver in Figure 4. Tubes with smaller outer diameter are preferred to maximise the allowable solar irradiance, however the sodium velocity constraint imposes a lower limit to the tube size.
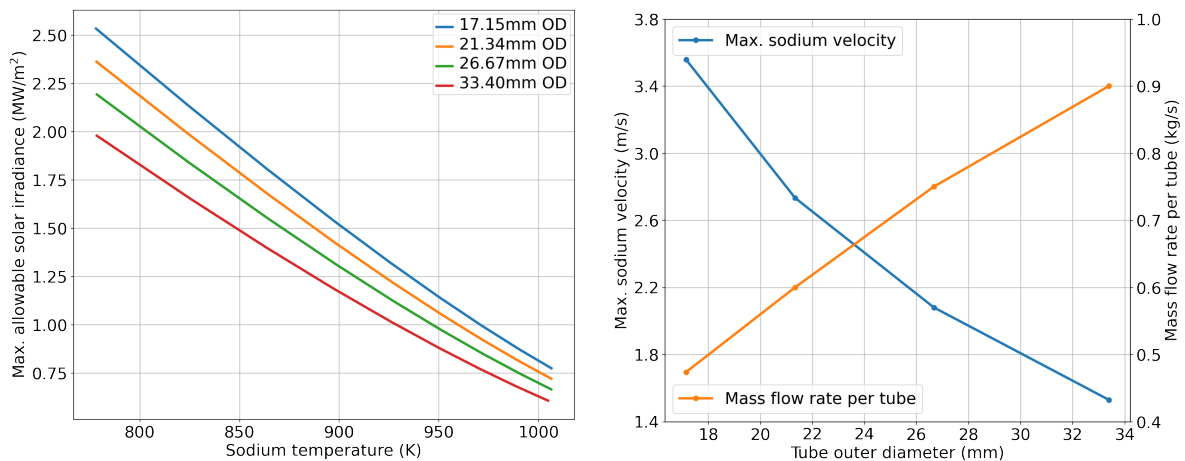


**Figure 4.** *Maximum allowable solar irradiance (left) and maximum sodium velocity (right) for a billboard receiver (11.7MWth capacity, 4.056 × 4.056m aperture, seamless 740H tubing).*

Potential receiver designs are first simulated in a detailed fashion with mesh-based energy balance equations [11]. This permits accurate assessment of the tube allowable flux and receiver performance, and subsequently for the receiver geometry design variables to be iteratively adjusted to meet design requirements (i.e. maximising efficiency whilst adhering to material limitations). Following the detailed receiver simulations and determination of appropriate values for the receiver design variables, a simplified aperture-based energy balance model is built for use in the SCS optimisation model. The parameters for the simplified model are solved for by curve fitting to the more detailed mesh-based simulations. It was found that the simplified model can is only in significant error for very low power conditions near sunrise and sunset.

## 2.3 Heliostat field modelling

Radially staggered and Cartesian heliostat field layouts are considered, Figure 5. The radially staggered layout pattern consists of an inner exclusion zone, a dense packing zone, and a series of radially staggered zones. The radially staggered heliostat field design is controlled by 7 parameters that determine the heliostat field capacity, the extents of the exclusion and dense zones, the initial and final azimuthal spacing, and the radial distance between rows and zones. The Cartesian layout pattern consists of straight rows and columns of heliostats with an inner exclusion zone around the tower. The spacing between rows and columns is allowed to increase as a linear function of distance from the tower position in each axis. The Cartesian heliostat field design is controlled by 5 parameters that determine the heliostat field capacity, extent of the exclusion zone, the spacing between columns (2 parameters) and spacing between rows. The exclusion zone radius is fixed at 25m, whilst the remaining pattern parameters are considered variables for optimisation.
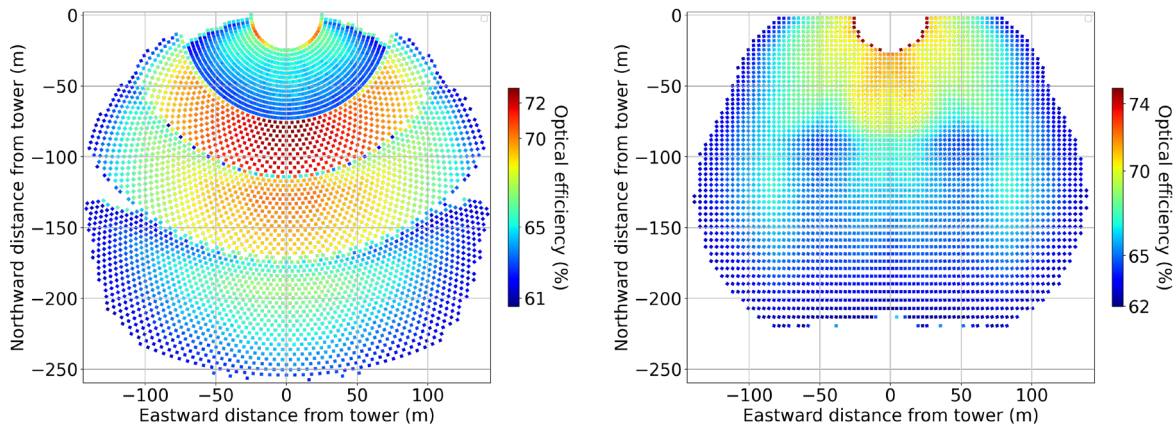


***Figure 5****. Examples of radially staggered (left) and Cartesian (right) heliostat field layouts for a billboard receiver on an 80m tower without boundary constraints.*

To minimise the land footprint and increase the packing density of the modules a rectangular boundary constraint can be imposed on the heliostat field designs, Figure 6. In the present work this boundary constraint was only applied for select cases as a manual post processing step. In future work, the rectangular boundary constraint could be parametrised and included as variables for optimisation.
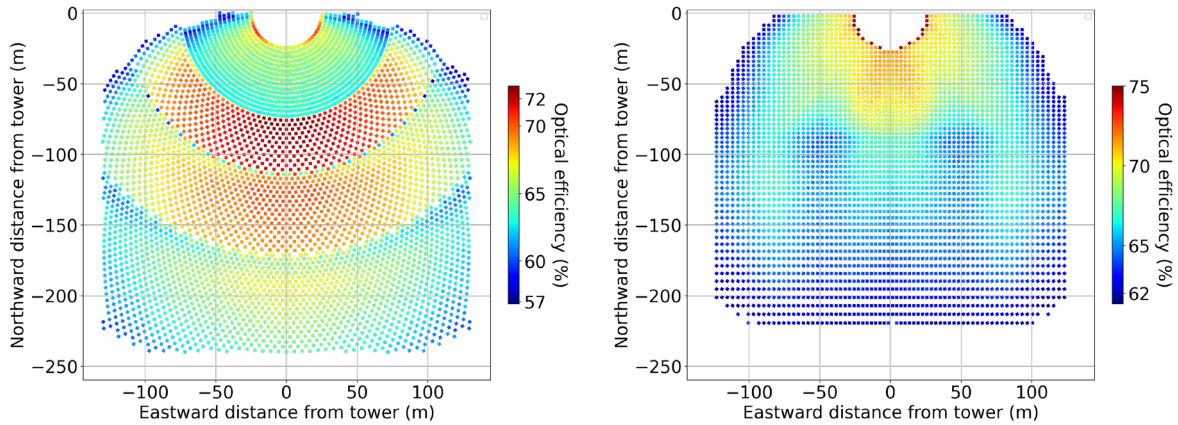
5

***Figure 6**. Examples of radially staggered (left) and Cartesian (right) heliostat field layouts for a billboard receiver on an 80m tower with boundary constraints.*

## 2.4 System optimisation

The objective function for optimisation of the SCS is the levelised cost of thermal energy captured by the receiver from a single tower module – here referred to as 'LCOH'. The available optimisation variables are the receiver geometry parameters, the heliostat field design parameters, and the tower height. The option exists for any of these variables to be set at fixed values to perform parameter sweeps and observe the resultant trends (e.g. LCOH as a function of tower height for a particular receiver design, as presented in the following section). The COBYLA algorithm from the NLopt library [12] as implemented in CSIRO's Workspace software [13] is used to minimise the objective function. A convergence tolerance of 0.001 is used and between 50 and 100 iterations are usually required to obtain a solution.

## 3. Results

Detailed investigations of the billboard and cavity receiver designs were first performed by parametrically varying the receiver design parameters with the tower height fixed at 50m tower and a radially staggered field considered. The tube bank design for both receivers were found to be driven by the tube stress constraint rather than performance – i.e., smaller tube banks would allow lower LCOH to be achieved but the resultant higher flux density was not within the limits for the 740H tubing. The receiver tube bank design parameters and receiver costs determined for both the billboard and cavity receiver variants are listed in Table 2. The billboard design was found to allow for substantially lower overall size of the tube banks compared to the cavity receiver, resulting in a similarly lower receiver capital cost. This is due to the use of the multi-aimpoint strategy for the billboard receiver permitting more accurate flux distribution on the tube banks, thereby making more efficient use of the costly 740H tubing.

***Table 2.** Receiver tube bank design parameters.*

| Receiver design | **Billboard** | **Cavity** |
|---|---|---|
| Tube banks per flow path | 3 | 5 |
| Tubes per bank | 30 | 28 |
| Tube OD (mm) | 21.34 | 21.34 |
| Tube length (m) | 4.056 | 4.4 |
| Angle between tube banks (°) | 180 | 168 |
| Cavity depth (m) | - | 2.75 |
| Total projected area of tube banks (m$^2$) | 16.5 | 27.8 |
| Receiver capital cost (USD/kW$_{th}$) | 93 | 164 |

These tube bank designs were then held constant, and the SCS optimised for each receiver and heliostat field design combination. LCOH and annual efficiency as a function of tower

6

height are plotted in Figure 7. Despite the cavity receiver offering increased efficiency for all cases, the LCOH for the billboard receiver is significantly lower due to the reduced receiver cost. For the billboard receiver cases the radially staggered field design is preferred at tower heights below 70m, however the overall lowest LCOH is achieved with the Cartesian heliostat field design at an optical tower height exceeding 80m.
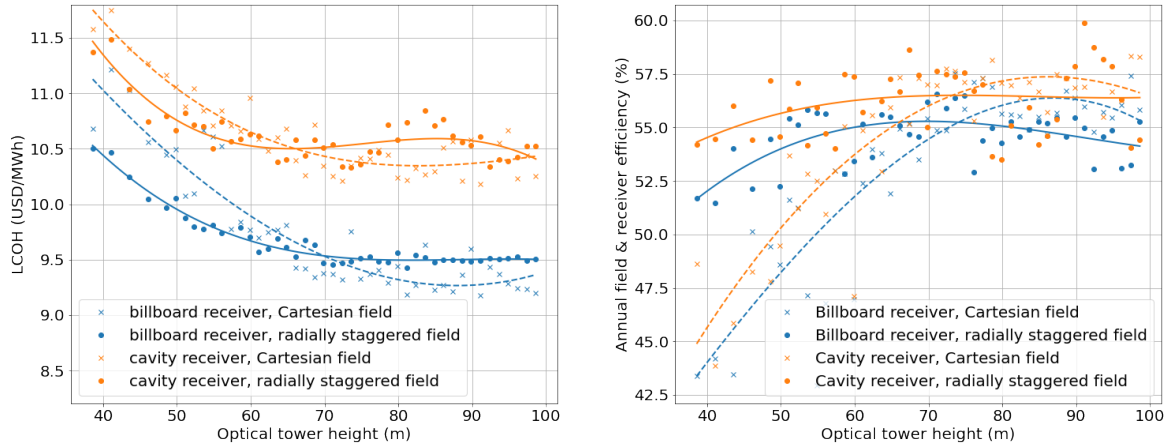


**Figure 7.** *LCOH (left) and efficiency (right) versus tower height.*

Two potential designs were selected for further investigation – 1) a billboard receiver on a short 50m tower with a radially staggered heliostat field, and 2) a billboard receiver on a tall 82.5m tower with a Cartesian heliostat field. Manually sized rectangular boundary constraints were applied to the heliostat field layouts, Figure 8, and were found to reduce the LCOH by approximately 2% for both designs. Although the Cartesian field with tall tower option has a significantly more compact land footprint and therefore lower pipe networking costs, the increased tower height also increases the average heliostat focal distance. This could be problematic for the high temperature sodium billboard receiver where it is important to be able to precisely control the flux distribution on the absorber tube banks by making use of tight heliostat images that can be aimed at specific areas.
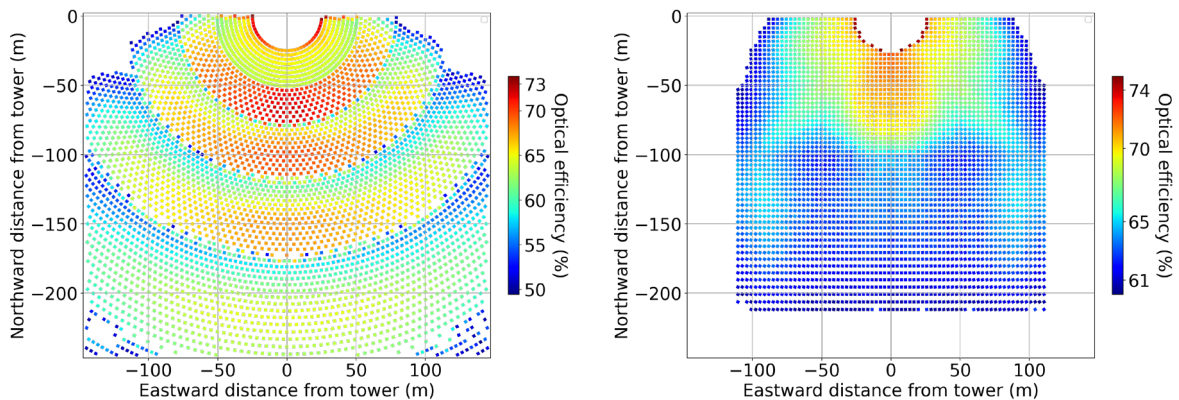


**Figure 8.** *Heliostat fields with rectangular boundary constraints for a billboard receiver on a 50m tower with a radially staggered layout (left) and on an 82.5m tower with a Cartesian layout (right).*

## 4. Conclusion

Optimised designs of 11.7MWth SCS modules based on high temperature (740°C) sodium central receivers have been investigated. Billboard and cavity receivers mounted on steel lattice towers have been considered, and radially staggered and Cartesian heliostat field layouts compared. A billboard receiver paired with a Cartesian heliostat field layout was found to give

the overall lowest levelised cost of heat (LCOH), albeit with a significantly taller tower compared to using a radially staggered heliostat field layout. Future work should seek to incorporate the rectangular land boundary constraint parameters into the optimisation model, and more closely integrate the SCS and plant models so that LCOE-based optimisation of all subsystems can be performed. An LCOE-based optimisation (as opposed to the LCOH-based optimisation presented here) would allow the approximation of a fixed pipe networking cost per heliostat field east-west extent to be avoided, and also allow the coupling between solar collection subsystem design and system design (e.g. pipe networking design, storage hours, power block size) to be investigated. Furthermore, the possibility of pairing Cartesian heliostat field layouts with shorter towers should be investigated as a multi-tower design with radially staggered layouts may not allow for convenient access by vehicle for the cleaning of heliostats.

## Data availability statement

Data will be made available upon request.

## Author contributions

Daniel Potter: Methodology, Formal Analysis, Investigation, Writing – Original Draft. Yen Chean Soo Too: Conceptualisation, Formal analysis, Investigation, Project administration, Supervision, Funding acquisition.

## Competing interests

The authors declare no competing interests.

## Funding

## References

1. C. Turchi et al., "CSP Gen3: Liquid-Phase Pathway to SunShot", Technical Report, National Renewable Energy Lab. (NREL), Golden, CO (United States), 2021, doi: 10.2172/1807668.
2. B. Leslie and K. Drewes, "Holistic optimisation of modular field design including heliostats, receivers, towers, HTF piping and operations," AIP Conf. Proc., vol. 2445, p. 120016, May 2022, doi: 10.1063/5.0089018.
3. C.-A. Asselineau, A. Fontalvo, S. Wang, F. Venn, J. Pye, and J. Coventry, "Techno-economic assessment of a numbering-up approach for a 100 MWe third generation sodium-salt CSP system," Solar Energy, vol. 263, p. 111935, July 2023, doi: 10.1016/j.solener.2023.111935.
4. J. Coventry, F. Venn, D. Potter, C.-A. Asselineau, W. Gardner, J.-S. Kim, W. Logie, R. McNaughton, J. Pye, and W. Stein, "Design and Construction of a 700kWth High-Temperature Sodium Receiver," in Proceedings of SolarPACES 2022.
5. D. Potter, J.-S. Kim, A. Khassapov, R. Pascual, L. Hetherton, and Z. Zhang, "Heliosim: An integrated model for the optimisation and simulation of central receiver CSP facilities," AIP Conf. Proc., vol. 2033, p. 210011, 2018, doi: 10.1063/1.5067213.
6. G. Zhu et al., "Roadmap to Advance Heliostat Technologies for Concentrating Solar-Thermal Power," Technical Report, National Renewable Energy Lab. (NREL), Golden, CO (United States), 2022, doi: 10.2172/1888029.

7.  P. Ingenhoven, L. Lee, W. Saw, M. Mujahid, D. Potter, and G. J. Nathan, "Techno-economic assessment from a transient simulation of a concentrated solar thermal plant to deliver high-temperature industrial process heat," Renew. Sustain. Energy Rev., vol. 185, 2023, doi: 10.1016/j.rser.2023.113626.

8.  A. Beath, M. A. Meybodi, and G. Drewer, "Techno-economic assessment of application of particle-based concentrated solar thermal systems in Australian industry," J. Renew. Sustain. Energy, vol. 14, no. 3, 2022, doi: 10.1063/5.0086655.

9.  J. E. Rea, C.J. Oshman, M.L. Olsen, C.L. Hardin, G.C. Glatzmaier, N.P. Siegel, P.A. Parilla, D.S. Ginley, and E.S. Toberer., "Performance modeling and techno-economic analysis of a modular concentrated solar power tower with latent heat storage," Appl. Energy, vol. 217, pp. 143–152, Feb. 2018, doi: 10.1016/j.apenergy.2018.02.067.

10. K. Tsuda, Y. Murakami, J. F. Torres, and J. Coventry, "Development of high absorption, high durability coatings for solar receivers in CSP plants," AIP Conf. Proc, vol. 2033, p. 040039, 2018, doi: 10.1063/1.5067075.

11. D. Potter, J. Kim, and R. McNaughton, "Simulation of a demonstration high temperature liquid sodium receiver with Heliosim," in Proceedings of the Asia Pacific Solar Research Conference, 2019.

12. S. G. Johnson, "The NLopt nonlinear-optimization package." http://github.com/stevengj/nlopt (accessed Oct. 12, 2023).

13. D. Potter, L. Hetherton, D. Thomas, R. McNaughton, and D. Watkins, "An integrated optimisation functionality for Workspace," MODSIM 2019, pp. 463–469, Dec. 2019, doi: 10.36334/modsim.2019.d2.potter.